Int. J. Electrochem. Sci., 16 **(2021)** Article ID: 210655, doi: 10.20964/2021.06.33

International Journal of
ELECTROCHEMICAL
SCIENCE
www.electrochemsci.org

Mini Review

A Review on Application of $LiFePO_4$ based composites as electrode materials for Lithium Ion Batteries

Yue-Ming Xin[1], *Hai-Yan Xu*[1,2,*], *Jun-Hai Ruan*[1], *Dong-Cai Li*[2], *Ai-Guo Wang*[1], *Dao-Sheng Sun*[1]

[1] Anhui Key Laboratory of Advanced Building Materials, Anhui Jianzhu University, Hefei, Anhui, 230022, PR China
[2] Key Laboratory of Functional Molecule Design and Interface Process, Anhui Jianzhu University, Hefei, Anhui, 230601, PR China
[*]E-mail: xuhaiyan@ahjzu.edu.cn

Received: 21 October 2020 / *Accepted:* 29 March 2021 / *Published:* 30 April 2021

Li-ion batteries have been put forward a huge demand for further developing rate performance and cycle stability. Under the new emerging industrial revolution and the accelerating pace of life, the addition of carbon in the electrode active material has been proven an effective way to improve its rate performance and cycle life. In the review, the current researches on the morphology of $LiFePO_4$, adding carbon, carbon sources and modified carbon (such as doping, ordered porous, etc.) on the performance of $LiFePO_4$ have been summarized. In general, the coating and mixing of carbon greatly promote the improvement of the rate performance and cycle stability of LIBs. The doping of various single element and multi-element atoms in carbon has great prospect for surface modification of electrode materials.

Keywords: derived carbon, $LiFePO_4$, rate performance, cycle life

1. INTRODUCTION

In the past few decades, the consumption of non-renewable energy was became seriously consumed with the fast development of the global productivity. The demand to petrol-powered cars is shifting to electric cars. Rechargeable batteries have become the most populative energy in contemporary society. Rechargeable lithium-ion batteries (LIBs), featured by light weight, high capasity density, high voltage and environmental friendliness, have applied on laptops and mobile phone, what' more, the vehicles also uses electricity due to their high specific energy and cycle stability. The commercialized Li-ion battery ($Li_xC_6/Li^+/Li_{1-x}CoO_2$ [1]) was first applied to electronic equipment by Sony Corporation in 1991. Now lithium-ion batteries are widely used all over

the world [2]. Huge advances that the anode of Li metal was replaced by graphite had been made in safety of LIBs. As is known to all, lithium metal as the anode material is more likely to produce lithium dendrite [3], which punctures the separator and causes the battery short circuit compared with the anode of graphite. Furthermore, graphite anode has reasonably low potential versus lithium. However, the cathode material has always been a limiting factor to LIBs. More and more researches focused on the ways to optimize the electrochemical performance of the cathode electrode. The crystal structure, morphology, size and modification of electrode material have attracted much attention to improve the cathode material performance.

As a stable, inexpensive and safe inorganic material, carbon has been used in various places because of high conductivity of graphene, various controlled morphology and wide source of raw materials. The addition of carbon is of great significance to the field of electrochemistry. In rechargeable LIBs, carbon materials are coated and mixed to modify the rate performance and cycle life of electrode materials. This review takes lithium iron phosphate as an example to review the effect of carbon materials in the performance of the cathode materials in LIBs.

$LiFePO_4$ (LFP) [4] has the obvious advantages of its olivine structure, such as high safety, environmental friendliness, nontoxic, and low cost. However, it also has poor electronic conductivity and slow lithium ion deintercalation speed during charging/discharging owing to non-continuous FeO_6 octahedral network to transmit electrons over Fe-O-Fe, and its one dimensional tortuous Li-ion channels [4]. Reducing particle size, designing LFP morphology and coating carbon on the surface of LFP have been well developed to improve the electrochemical performance of LFP [5]. Carbon coating is the best mode to modify lithium iron phosphate at present. It is beneficial to optimize the electronic conductivity of the material [6] and the rate performance. Moreover, reduction of the particle size of LFP [7,8] is also a successful way to optimize its electrochemistry performance. Different carbon sources and morphologies show different characteristics [9-13].

In the review, the current researches on LFP have been summarized in light of above technical challenges. The structural characteristics, morphological features and the electrochemical performance of various LFP/C with different carbon sources have been reviewed and compared, as shown in Figure1. In addition, the capacity storage mechanisms of different carbon-based composite electrodes of LFP/C have also been described.

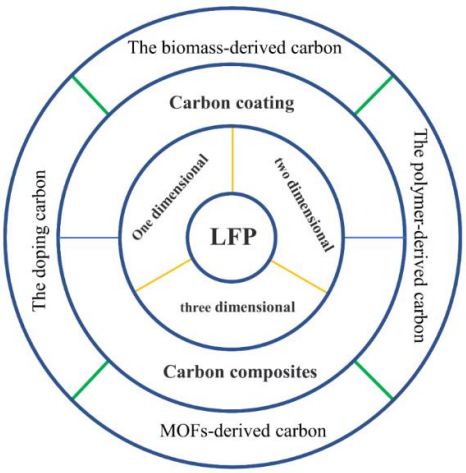

Figure 1. The Schematic diagram of the morphology of LFP and carbon addition

2. ENERGY STORAGE MECHANISMS

2.1 Structural features

The olivine lithium iron phosphate consists of distorted FeO_6, LiO_6, and PO_4 units, and The olivine lithium iron phosphate consists of distorted FeO_6 octahedra, LiO_6 octahedra, and PO4 tetrahedron units, and the absence of continuous FeO_6 octahedral connections results in low electrical conductivity [14]. Therefore, the olivine compound displays lower electrical conductivity. The 3D delocalized chemical bond of LFP is formed by a strong P-O covalent bond, so LFP has thermodynamic and dynamic stability even at temperatures higher than 200°C.

2.2 Electrode features

The energy transfer mechanism of LFP is the insertion/extraction of Li^+ in the active material. During charging, the Li^+ enter the cathode material from the electrolyte and lithium metal in the negative electrode loses electrons to form Li^+ that diffuses into the electrolyte to keep the charge balance of the electrolyte host materials. Discharge is the opposite (Figure 2) [15]. LFP cathodes and C anodes can be formulated as follows:

Anode: $C_6Li - xe \rightleftarrows C_6Li_{1-x} + xLi^+$ (1)

Cathode: $Li_{1-x}FePO_4 + xLi^+ + xe \rightleftarrows LiFePO_4$ (2)

Overall: $C_6Li + Li_{1-x}FePO_4 \rightleftarrows C_6Li_{1-x} + LiFePO_4$ (3)

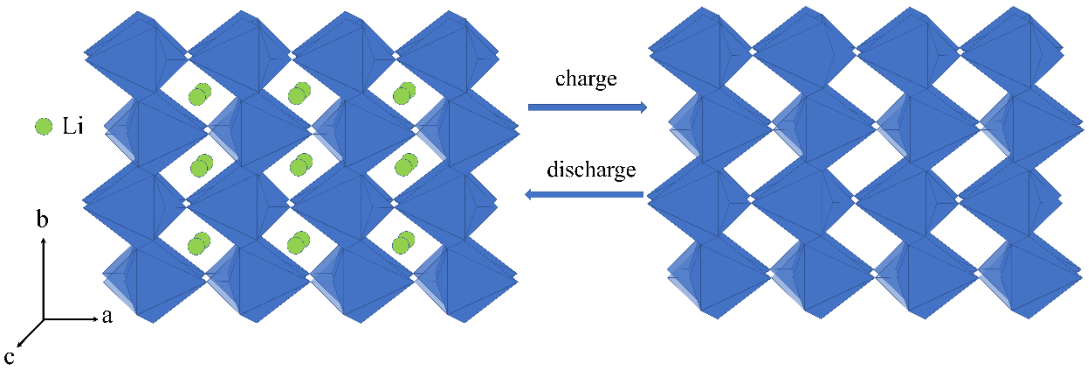

Figure 2. Olivine structures of LFP and $FePO_4$ phase removed Lithium.

There are both faraday process and pseudocapacitive faraday process in LFP/C. In cyclic voltammetry, the relationship between current i and scan rate v usually reflects the pseudocapacitive faraday process ($i=av^b$ [16], where a and b are adjustable parameters, suitable for single electron system). When the value of b is 0.5, ion diffusion dominates the entire electrochemical process. However, when the value of b increases to about 1, the charge and discharge process is mainly controlled by the pseudocapacitive faraday process. The larger the value of b, the higher the

pseudocapacitive capacity, and the faster the charge transfer speed, resulting in a better rate capability. In order to further explore the electrochemical reaction kinetics, the contribution of faraday and non-faraday currents to the overall reaction can be calculated according to the following formula (4) by Dunn's group[17-20].

$$I_p/v^{1/2} = k_1 v^{1/2} + k_2 v \quad (4)$$

For example, Kisu and co-workers [21] found that the high rate capability was owing to the existence of Fe^{3+} in the surface of LFP crystal structure. The fast pseudocapacitive process explained the high rate performance of the LFP/graphitic carbon composite, and 25% of the total capacity is mainly contributed by it. Guan et al. [22] synthesized LFP coated with activated carbon and graphene. The specific capacity retained 66 $mAh \cdot g^{-1}$ at 100 C due to a 3D carbon network built to deliver capacitance.

3. THE MORPHOLOGY AND RATE CAPABILITY OF LFP

In this section, the influence of morphology of LFP on the rate capability is going to be introduced. The rate capabilities of one-dimensional, two-dimensional, three-dimensional LFP are going to be discussed in detail.

3.1 One dimensional LFP

According to Lim's work [23], the one-dimensional (nanowire and nano hollow wire) $LiFePO_4$ cathodes were synthesized using the hard templates KIT-6 and SBA-15. The electrochemical cycling performance test of one dimensional LFP cathodes showed fantastic rate performance (89% of the initial capacity is retained) even at 10 C. The rate capability of the nano hollow wire cathode at 15 C was 6 % higher than that of the nanowire cathode because of its higher specific surface area [24].

Huang et al. [25] synthesized 1D LFP nanorods through a facile hydrothermal process at 220 °C for 18 h. The nanorods with a preferred orientation along b axis were beneficial to transport lithium ions. The 1D LFP nanorods delivered a discharge specific capacity of 132 $mAh \cdot g^{-1}$ at 0.5 C after 20 cycles.

Liu et al. [26] synthesized LFP nanorods using $FePO_4$ nanorods as the raw material. The pre-synthesized $FePO_4$ nanorods, $LiOH \cdot H_2O$, and polyethylene glycol (PEG: The average molecular weight is 10,000, 250g PEG/mol $FePO_4$) powders were mixed completely in an agate mortar, heated at 700 ^oC for 8h under flowing nitrogen, and then the final product was obtained when the temperature dropped to room temperature. 150, 141, 94 and 80 $mAh \cdot g^{-1}$ were the first discharge capacities at the 5, 10, 50 and 60 C, respectively. The Coulomb efficiency remains above 98 %.

Ma et al. [27] synthesized nanorods with rectangular prisms and hexagonal prisms by a solvothermal process in glycerol and water system. The LFP with the rectangular prism nanorod morphology has better advantages in electrochemical performance. The nanocrystalline grain size and more exposed (010) crystal planes greatly shorten the migration path of Li^+ inside the LFP. At a low

rate of 0.2C, it has 96.4%(163.8 $mAh \cdot g^{-1}$) of the theoretical capacity of LFP. When the rate was increased by 100 times to 20C, 75 $mAh \cdot g^{-1}$ could be retained, and the coulombic efficiency remains stable.

To sum up the description of the electrochemical performance of one-dimensional lithium iron phosphate with the addition of carbon, the capacity and rate performance were improved. Based on the results mentioned above, the relative capacity of LFP coated with carbon at 5 C reported by Liu was 14 % higher than that of LFP electrode without carbon at 0.5 C reported by Huang. Even the rate was increased up to 10 C, the former capacity still retained 7 % higher than the later one at 0.5 C.

3.2 Two dimensional $LiFePO_4$

LFP nanosheets with a single crystal plane (010) are synthesized by Zhao et al. [28], which provided the highest ion channel for lithium-ion insertion/extraction by charge/discharge. The two dimensional LFP delivered a high specific discharge capacity of 120, 85, and 72 $mAh \cdot g^{-1}$ at the 5, 10, and 20C, respectively, although the nanosheets exhibited normal capacities, 151 and 140 $mAh \cdot g^{-1}$ at 0.5 C and 1 C. Due to the shorter lithium ion diffusion distance of the two-dimensional LFP, it exhibits excellent rate performance during charging and discharging.

The rate performance and cycle life of 2D LFP cathode coated with carbon can be further increased, compare with the above-mentioned bare 2D LFP electrode.

Zhang et al. [29] synthesized LFP microplates with exposed (010) faces by a solvothermal approach. After coated carbon, the LFP/C microplates delivered the first discharge capacity at 0.1 C was 157 mAh·g-1. Increasing the current density to 10 and 20 C could still maintain 63.7% and 51.6% of the first discharge capacity, respectively. After 100 cycles at 1C and 5C rates, there was still no obvious capacity degradation, the reversible discharge capacities remained approximately 139 and 118 $mAh \cdot g^{-1}$, respectively. The capacity under 10 C and 20 C increased by 17.6 % and 12.5 %, respectively, compared with the above result of Zhao et al.

Zou et al. [30] prepared LFP nanosheets with abundance (010) faces and extremely low antisite defect with SA (sodium alginate)/r-GO (reduced graphene oxide) assisted. They obtained a multilayered structure which was formed by Van der Waals forces and hydrogen bonds between the Li-Fe-P-alginate molecules and 2-dimensional r-GO nanosheets. The LFP-NS/r-GO cathode exhibited a capacity of 98.6 $mAhg^{-1}$ at 100 C. The reversible capacity of LFP-NS/r-GO-10 (10, mass ratio (%) of r-GO/SA) retained 130.6 $mAh \cdot g^{-1}$ at the C-rate of 10 after 2000 cycles and the capacity was 99.55% of the initial discharge capacity. It was far higher than above work of Zhao et al (90 $mAh \cdot g^{-1}$ after 1000 cycles at 10 C).

3.3 Three dimensional LFP

It is well known that controllable the b-axis of LFP is the rapid diffusion channels to the lithium ions. Kim [31] reported 3D porous microsphere LFP by a supercritical and spray-dry combination method. Controlling the direction of crystal growth is considered to be a promising

method to greatly increase the transfer efficiency of Li^+ [32]. The porous LFP reported by Kim with high contact area with electrolyte and high tap density (1.7 $g \cdot cm^{-3}$) displayed abundant 3D channels, which was beneficial to reduce the resistance of the contact between the electrolyte and the electrode, and improved the diffusion performance of lithium ions. The optimized 3D LFP composite with carbon coating (3.3wt.%) displayed remarkable electrochemical performances of a high specific capacity (153.4 $mAh \cdot g^{-1}$ at 0.2 C) and a high rate performance (133.7 $mAh \cdot g^{-1}$ at 1 C). The porous 3D $LiFePO_4$ is generally coated with carbon to improve its conductivity. Goodenough'group [33] reported 3D porous microspheres flower-like LFP/C, to which polypyrrole (ppy) was attached through polymerization reaction to further improve its rate performance. Because of its good crystallinity and conductivity, there were still 110 $mAh \cdot g^{-1}$ and 86 $mAh \cdot g^{-1}$ at the C-rate of 5 and 10 after 1000 cycles, respectively. Table 1 summarizes the synthesis method, crystal morphology and specific capacity based on the literature of LFP preparation in recent years.

Table 1. The relationship between morphologies and capacities

Materials	Preparation	Performances	Ref.
Nanowire and hollow $LiFePO_4$	Templates method	147 $mAh \cdot g^{-1}$ at15C	[23]
Nanorods $LiFePO_4$	Annealing+hydrothermal process	122$mAh \cdot g^{-1}$ at 5C	[34]
Nanorods $LiFePO_4$	Heat method	80 $mAh \cdot g^{-1}$ at 60C	[26]
Rectangular prism nanorod $LiFePO_4$@C	Solvothermal method	75 $mAh \cdot g^{-1}$ at 20C	[27]
Nanosheets $LiFePO_4$	Solvothermal method	72 $mAh \cdot g^{-1}$ at 20C	[28]
Microplates LiFePO4/C	Solvothermal method	81 $mAh \cdot g^{-1}$ at 20C	[29]
Ultrathin nanosheets $LiFePO_4$	Sol-gel method	98.6 $mAh \cdot g^{-1}$ at 100C	[30]
3D porous microspherical $LiFePO_4$/GA	Hydrothermal method	115 $mAh \cdot g^{-1}$ at 10C	[35]

Due to the unique one-dimensional ion channel of LFP, the above researches achieved rapid ion extraction and insertion to improve its rate performance through shortening the [010] directional path of the ion channel by various methods. However, the internal electronic conduction characteristics of LFP limited by its own structure decide that the electronics can only migrate along the Fe-O-Fe direction [36]. Unfortunately, there is no continuous FeO_6 octahedral network in the structure at all. At this point, the rate performance of the low-dimensional LFP cathodes is definitely limited to its poor electronic conductivity. The three dimensional porous materials in this aspect can provide more Li-ion channels owing to the close contact with electrolyte, and relatively lower charge transfer resistance [37]. It means that less channel-clogging defects in 3D porous LFP particles result in high capacity [38]. However, no matter how the morphology is tailored, the rate performance of LFP is still far away from the ideal. Therefore, modification of LFP is urgently required to further improve the electrochemical performance.

4. THE EFFECTS OF CARBON ON LFP BASED COMPOSITES

Recently, there are more and more reports on LFP-carbon cathodes. On the one hand, different sources of carbon, such as biomass [39], polymer, and MOFs [40], have been investigated to prepare carbon coated LFP cathodes. On the other hand, carbon materials with various morphologies, including carbon nano tubes, graphite sheets and so on, have been used to obtain LFP/carbon composite cathodes. The related performance parameters of LFP cathodes coated with carbon are showed in Table 2.

Table 2. The related performance parameters of LFP cathodes coated with carbon

Carbon thickness (nm)	Max capacity ($mAh \cdot g^{-1}$)	I_D/I_G	Diffusion coefficient ($cm^2 \cdot s^{-1}$)	R_{ct} (Ω)	BET ($m^2 \cdot g^{-1}$)	Pore size (nm)	Ref.
2.8	150	0.9		190	13.6	15.5	[41]
3.5	165	0.89		120	20.4	16.4	[41]
	168		4.73×10^{-13}	112	268.95	5	[35]
	151.1	1.18	1.17×10^{-13}	350	43.45	3-4	[42]
	169.3	1.12	1.07×10^{-12}	137	92.75	0	[42]
2.4	165		8.72×10^{-12}	57.08			[43]
	162	0.872			91	3-30	[44]
1-2	161.5	0.89		74.2			[45]
10	139		1.06×10^{-11}	216	85.953	3.42	[46]
	162	1.04	9.06×10^{-11}	289	90.92	10	[47]
20-30	163	1.08	2.16×10^{-12}	103	197.2		[48]
3	155.5		9.05×10^{-12}	265.5			[49]

4.1 LFP/C composites

Table 3. The performance of LFP/carbon cathodes from different carbon precursors

Carbon types	Performances (0.1C)
Amorphous Carbon	150.3 $mAh \cdot g^{-1}$
Carbon nanotubes+ Amorphous Carbon	155.7 $mAh \cdot g^{-1}$
Graphene+ Amorphous Carbon	159.7 $mAh \cdot g^{-1}$
Amorphous Carbon+ Carbon nanotubes+ Graphene	164.5 $mAh \cdot g^{-1}$

Cai et al. [50] synthesized high performance LFP cathode materials using amorphous carbon (C), carbon nanotubes (CNTs), and graphene (G) as conductive materials via sand milling and spray

drying processes and followed by calcination. The performances of LFP/carbon cathodes from different carbon precursors are listed in Table 3.

By adding graphene and carbon nanotubes to LFP/C, the charge transfer resistance was reduced from 248Ω (LFP/C) to 50Ω, and the charge transfer resistance was reduced by 80%. The initial columbic efficiency of LFP/C/G/CNTs (96.5 %) was 5 % higher than that of LFP/C (91.9 %).

Graphene has drawed much attention owing to its high specific surface area, high theoretical capacity and good mechanical properties [51, 52]. However, it's quiet hard to achieve dispersion in homogeneity. It has been confirmed that adding carbon nanotubes to graphene is beneficial to enlarge the spacing between graphene sheets to avoid aggregation[53].

So far, mixed LFP with 1-dimensional (1D), 1-dimensional(2D), or 3-dimensional (3D) carbon as electrodes for Li-ion battery have been synthesized.

Du et al. [35] prepared 3-dimensional porous microspherical LFP/graphene aerogel (LFP/GA) composite for LIBs by one-step hydrothermal. In composite materials, graphene sheets were entangled together to form a three-dimensional network frame due to van der Waals forces and hydrogen bonds. Three-dimensional microspheres of LFP were composited on the frame. The graphene frame improves the electronic conductivity and lithium ion migration rate. The optimized LFP/GA composite displayed a excellent electrochemical performance of a high specific capacity (168 $mAh \cdot g^{-1}$, 0.1 C), 14 % higher than that of pure LFP (147 $mAh \cdot g^{-1}$, 0.1 C). The charge transfer resistance dropped from 664Ω(LFP) to 112Ω (LFP/GA). The Li^+ diffusion coefficient ($D/cm^2 \cdot s^{-1}$) of LFP/GA was 4.73×10^{-13}, much higher than that of LFP (8.88×10^{-14}). LFP/GA also showed a high rate performance (115 $mAh \cdot g^{-1}$, 10 C), and a high capacity retention (96.3 % even after 800 cycles at 1C).

In Huynh's work, using the hydrothermal method, the carbon nanotubes and the electrode material were combined to obtain LFP/C/10%CNTs, which aimed to improve the electrochemical performance of the electrode [54]. After charging and discharging tests, LFP/C/10%CNTs as an electrode active material released 190 $mAh \cdot g^{-1}$ at a rate of 0.1C after 200 cycles. The diffusion coefficient of LFP/C/10%CNTs (8.29×10^{-11}) increased 72 % than that of LFP/C (D-glucose) (2.28×10^{-11}). Carbon nanotubes also can store energy [55-57]. Therefore, the capacity of the composite material of LFP and carbon was larger than the theoretical capacity of LFP.

Wu and co-workers [58] reported that integrating the advantages of porous carbon and active particles (LFP) at the nanometer scale. The composite electrode materials of excellent electrochemistry performance were obtained by dispersing LFP nanoparticles into nanoporous carbon .Complete charge and discharge in less than 30 seconds, in the first 15 cycles, at the rate of 0.9C, the specific capacity gradually increased and finally stabilized at 145 $mAh \cdot g^{-1}$. The power density increased by about 50 times (from 38 $Wk \cdot g^{-1}$ to 1875 $Wk \cdot g^{-1}$), its capacity still retained about 60 % (from 145 $mAh \cdot g^{-1}$ to 85 $mAh \cdot g^{-1}$).

Long and co-workers [10], synthesized a novel c-LFP/graphere in which LFP/C nanorods embedded in a matrix built of interweaved graphene nanosheets. The electronic conductivity of C-LFP (5.6×10^{-5} S·cm) increased 2.5×10^3 than that of C-LFP/graphene (1.39×10^{-1} S·cm).The surface of LFP nanorods was coating carbon film, which size was about 1.5-2.0 nm. It delivered 100 $mAh \cdot g^{-1}$, 80 $mAh \cdot g^{-1}$ at 20 C ,50 C, respectively and preserved a high tap density of 1.76 $g \cdot cm^3$.

4.2 The carbon coating

4.2.1 The biomass-derived carbon

Xu et al. [49] demonstrated a Simple one-step synthesis route to coated LFP particles with nitrogen-doped graphite carbon (NGC). The coated carbon layer was about 3 nm. They used chitosan successfully obtained the nitrogen-doped carbon through the method of freeze-dried and annealed. It delivered a specific capacity of ~ 155.5 mAh·g^{-1} with columbic efficiency ~ 97 % at 0.1 C, 63.2 mAh·g^{-1} at 5 C, and columbic efficiency and capacity retention ratio ~ 100 % after 100 cycles. LFP@NGC cathodes reduced the resistance by 80 % from 1343.0 Ω (LFP) to 265.5 Ω. The calculation results from Eq. (5) showed that The LFP @ NGC cathode increases the lithium ion diffusion coefficient by (9.05×10^{-12} cm^2·s^{-1}) 2000 times than that of the LFP cathode (4.24×10^{-15}cm^2·s^{-1}).

$$Z_{real} = R_e + R_{ct} + \sigma\omega^{-1/2} \quad (5)$$

Different precursors of biomass have been investigated on LFP by Xiao et al. [59] In the report, α-D-glucose (αDG), pyromellitic anhydride (PA), soluble starch (SS), citric acid (CA), polyacrylamide (PAA) and sucrose (SC) were chosen as carbon precursors. The precursors of carbon and LFP were ball-milled, and then heated in an inert atmosphere. The capacities of carbon coated LFP from different carbon precursors are listed in Table 4.

Table 4. The capacity of different carbon precursors with LFP

Carbon source	Preparation	Performances(0.1C)	Ref.
Chitosan	Freeze drying technology and annealing	155.5 mAh·g^{-1}	[49]
α-D-glucose	Ball-milled+ sintered method	138mAh·g^{-1}	[59]
Pyromellitic Anhydride	Ball-milled+ sintered method	131mAh·g^{-1}	[59]
Soluble starch	Ball-milled+ sintered method	140mAh·g^{-1}	[59]
Citric acid	Ball-milled+ sintered method	148.3mAh·g^{-1}	[59]
Polyacrylamide	Ball-milled+ sintered method	95.4mAh·g^{-1}	[59]
Sucrose	Ball-milled+ sintered method	153mAh·g^{-1}	[59]
Fructose	Hydrothermal treatment	98 mAh·g^{-1}	[11]
Glucose	Carbothermal reduction + sintering method	159.3mAh·g^{-1}	[60]

In a similar report, Pratheeksha and co-workers [11] investigated in-situ carbon coated LFP with different carbon sources (glucose/ sucrose/fructose). The raw materials were dissolved in ethanol solution followed by hydrothermal treatment at 180°C to obtain carbon coated LFP. The carbon coated LFP from fructose (called C-LFP-F) showed better electrochemical performance in terms of energy

density and long cyclic, compared with carbon coated $LiFePO_4$ from glucose (called C-LFP-G) and sucrose (called C-LFP-S). The carbon layer of C-LFP-F was about 5nm, while that of C-LFP-G was too thickness, and the layer of C-LFP-S was discontinuous. C-LFP-F delivered a discharge capacity of 98 $mAh \cdot g^{-1}$, 48 $mAh \cdot g^{-1}$at 0.1 C , 1 C , respectively.

Liu et al. [60] prepared LFP/C by a carbothermal reduction method, and the glucose was used as carbon source by sintering. The particle size of lithium iron phosphate got smaller with the more amount of carbon content. It delivered a high capacity of 159.3 $mAh \cdot g^{-1}$ at 0.1C, and the capacity decreased about 2.2 % after 30 cycles.

Wi et al. [61] reported a porous-carbon/LFP nanocomposite by sol-gel process and the citric acid was used as the carbon network source. The LFP was coated by porous carbon and the pores were filled with electrolyte. On the view of the authors, the best performance of electrochemical was a carbon content of 13.7 wt %, which thickness was about 2.0 nm. At 5 C, it delivered a capacity of 96 $mAh \cdot g^{-1}$. In previous report [62], the BET surface of about 25 nm-size LFP nanoparticles was about 7 $m^2 \cdot g^{-1}$, while the BET of porous carbon/ $LiFePO_4$ of this article was 92 % larger than that reported in Ref. 62.

In general, biomass is a kind of convenient and easy carbon source to achieve carbon coated LFP, and the coating method is simple, safe, and environment friendly.

4.2.2 The polymer-derived carbon

Mo and co-workers [63] constructed a unique core-shell architecture to overcome the disadvantages of conventional LFP material, like low electronic conductivity, poor Li^+ diffusion coefficient and so on. The specific resistivity of the LFP@PAB-C (1, 3-diethynylbenzene-derived carbon) with continuous PAB-C layer was as low as ~ 0.01 Ω·cm, and the carbon layer was only 2.5 nm. Even at a considerable discharge rate of 50 C after 200 cycles, the capacity was still remained at 120.2 $mAh \cdot g^{-1}$, which was 88 % higher than that of LFP@GC (carbon from glucose), owing to its core-shell architecture. Meanwhile, the LFP@PAB-C nanocomposites also showed excellent long cycling stability, and the capacity remained about 100.6 % at 20C after 1000 cycles.

Zhou et al. [64] synthesized LFP/C by carbothermal reduction method using polystyrene (PS) spheres as carbon source. With the addition of carbon content increased, the particle sizes of LFP/C reduced from 1 μm to 0.2 μm. The electrochemical performance of LFP-3.0%C (carbon content was 3.0 % wt) was the best and delivered 147 $mAh \cdot g^{-1}$ at 0.1C. It presented a homogeneous coating with a thickness of 2.5 nm.

The performances of lithium iron phosphate are related to not only its own morphology and crystallization degree, but also the thickness of coating carbon film [65], carbon source, pore size and degree of graphitization of carbon. Cho et al. [66] investigated the relationship between carbon thickness and capacity, as shown in Table 5.

The thickness of the membrane to a certain extent determined the capacity of the lithium iron phosphate. Greater than 2V [67], carbon almost could not allow any lithium ion cross, as it became a

natural barrier between lithium iron phosphate and electrolyte [38]. At this point, the ion migration rate limited the LFP capacity and led to the battery polarization, internal resistance increase, and severe self-depletion.

In summary, the performance improvement of single factor of morphology is not satisfactory yet so far. The combination of carbon addition and morphology controlling can build a better conductive network. Moreover, the degree of graphitization of carbon also affects its performance [68]. The higher the degree of graphitization, the lower the charge transfer resistance [50]. The dense graphitized carbon layer can protect the electrode from the electrolyte in some certain extent, but it also becomes a barrier against the free diffusion of lithium ions. Therefore, it is very important effective controlling the graphitization and thickness of the surface carbon coating. Some of the data on the degree of graphitization are showed in Table 6.

Table 5. The comparisons of the conductivity, carbon content, carbon thickness, and discharge capacity of samples.

Materials	Electronic conductivity ($S \cdot cm^{-1}$)	Carbon content (wt.%)	Carbon thickness (nm)	Discharge capacity ($mAh \cdot g^{-1}$)	Synthesis condition
Pure $LiFePO_4$	5.88×10^{-8}	0.02	0	7th=99	873k 12h
Product-0	6.42×10^{-4}	1.25	2-6	7th=137	
Product-1	6.99×10^{-4}	1.67	2-15	7th=141	
Product-2	7.11×10^{-4}	2.28	4-8	7th=151	
Product-3	8.76×10^{-4}	2.54	10-25	7th=143	

Table 6. The effect of carbon

Carbon content (wt%)	Discharge capacity ($mAh \cdot g^{-1}$)	I_D/I_G	R_{ct} (Ω)	Ref.
9.3	165	0.89	120	[41]
4.7	150	0.9	190	[41]
6.2	163	1.08	103	[48]
6.89	169.3	1.12	137	[42]
7.48	151.1	1.18	350	[42]

4.2.3 MOFs-derived carbon

Due to the great advantages of carbon materials, optimizing MOFs-derived nanoporous carbon materials (the nanoporous carbons successfully gained by carbonization of MOFs under high

temperature annealing) has attracted more and more attention. A stable porous structure can be obtained from MOFs derived carbon, which can meet the needs of electrochemical applications and the preparation method is generally convenient and cheap [23]. Introduction of MOFs-derived nanoporous carbon will greatly improve electrical conductivity of LFP.

Xu et al. [69] reported a method to obtain LFP/C_{ZIF-8} by in-situ growth ZIF-8 on commercial LFP and then carbonization of the ZIF-8. The graphite-like carbon layer with metal zinc on the surface of the samples was approximate 10 nm thick. The discharge capacity and energy were 159.3 $mAh \cdot g^{-1}$ at 0.1 C, 141.7 $mWh \cdot g^{-1}$ after 200 cycles at 5.0 C, respectively (the capacity remained about 99 %). The performance optimization was mainly owing to the ZIF-8 derived porous graphite-like carbon layer on the surface of LFP. The LFP/C_{ZIF-8} had a hierarchical pore structure (size distribution in 1.9-244.7 nm). The interlaced hole structure was beneficial for electrolyte wetting, charge transfer, lithium ion diffusion (shorten the path of mass and charge transfer) and volume change of higher degree of freedom during electrochemical reaction cycle like charge, discharge and so on. The working mechanism of the coating layer of the LFP/C-ZIF-8 cathode materials was that the ions passed through the holes on the carbon coating layer to achieve mass transfer, and then the electrons achieved electricity transfer along the coating layer. Larger holes made up for the shortcomings of traditional carbon coatings that were relatively dense and affected the entry of electrolyte and subsequently affected ion transmission. The lithium diffusion coefficient of LFP/C ZIF-8 cathode (1.1708×10^{-13} $cm^2 \cdot s^{-1}$) was about 20 times higher than that of LFP cathode ($6.7553 \times 10^{-15} cm^2 \cdot s^{-1}$). Moreover, the R_{ct} of LFP/C_{ZIF-8} (188.9 Ω) was 57% less than that of the bare LFP (439.3 Ω).

Liu et al. [70] synthesized a porous hierarchical composite (LFP/CNWs) of LFP combined with MIL-100 derived carbon networks. MIL-100 was used as iron source to generate lithium iron phosphate in situ, and the ligand was carbonized and coated. The porosity of the CNWs gave the LFP a larger specific area, so as to better contact with the electrolyte. The LFP/CNWs with electrical conductivity of 6.01×10^{-2} $S \cdot cm^{-1}$ delivered remarkable specific capabilities of 158.1 and 80.4 $mAh \cdot g^{-1}$ at 0.1 C and 20 C, respectively.

There are plenty of types of MOFs, porous, varied in shape and diverse in center ions [71]. It is highly reasonable to believe that it is feasible using MOFs' central ions as a raw material to directly obtain interesting porous electrode materials by an in-situ synthesis method, in addition to using MOFs material to achieve a porous electric coating on the electrode material that can assist both matter and charge to transfer. For example, MIL-100(Fe) could be used as an iron source to synthesize porous lithium iron phosphate.

4.2.4 The doping carbon

Using biomass and MOFs carbon source is convenient to realize in-situ doping carbon with heteroatoms (e.g., Boron, Phosphorus, Sulfur, and Nitrogen) by a simple treatment process, then the electrochemical performance of the LFP/C electrode has been further optimized.

In recent years, the doping carbon has been widely investigated. Among all the heteroatoms, N is the element that attracted the most attention of researchers. Its atomic radius is similar to carbon atoms which can more easier to achieve doping[72]. The possible presence forms of nitrogen in carbon

materials include pyridinic N [73], pyrrolic N [74], oxidized pyridinic N [75], and quaternary N [75] as shown in Figure 3. Some MOFs (ZIF-8, ZIF-67, etc.) can also obtain heteroatom-doped porous carbon materials by in-situ calcination process owing to their containing heteroatoms (like N) [76, 77]. Sulfur atom has greater electronegativity and atomic radius than N atom, as the result, the structure defects of the carbon framework and the free electrons are all remarkably increase [78]. Therefore, both of the electron conductivity and ion diffusion are greatly improved. The reported advantages of doping carbon layer are as follows.

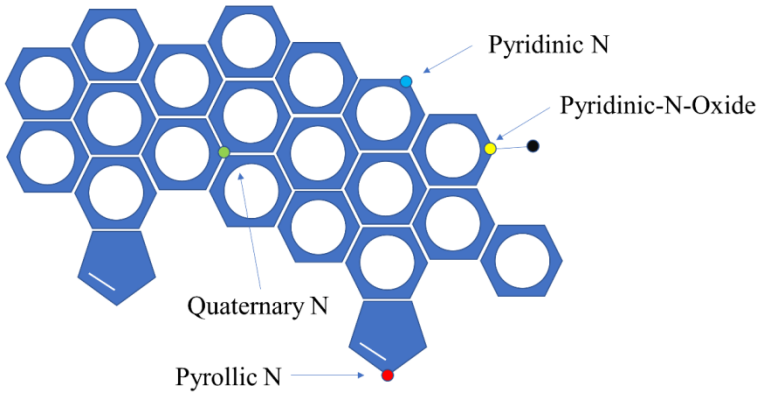

Figure 3. Possible forms of nitrogen in the carbon skeleton

i. A amount of defects in the carbon structure of sp^2 by nitrogen-doping are contribute to Li^+ diffusion in the interface [79].

ii. The electrnic conductivity in electron device can be remarkably increased by nitrogen-doped carbon [80, 81].

As mentioned above, Yuanyuan Liu et al. [70] coated an N-doped carbon layer on the LFP. The N-Carbon decreased the R_{ct} from 62.4 Ω to 52.7 Ω. The N-doped carbon coated LFP electrodes delivered super discharge capabilities of 161.5 and 93.6 $mAh \cdot g^{-1}$ at the C-rate of 0.1 and 20 respectively, 16.4% and 2.1% more than non-N-doped carbon layer. Xu et al. [49] reported that LFP@NGC cathodes reduced the resistance by 80 %, and the lithium diffusion coefficient was 2000 time larger than bare LFP. Ou and co-workers [82] obtained N-doped carbon from egg white. The R_{ct} value for LFP@ N-doped carbon was 20.5 Ω less than bare LFP. At the charge and discharge processes, the Li^+ diffusion coefficients for LFP@N-doped carbon were estimated to be 1.66×10^{-10} and 1.23×10^{-10} $cm^2 \cdot s^{-1}$, respectively.

For other dopants, phosphorus can produce the highest electron modulation efficiency. Because of P atom has lower electronegativity by it has lone pair electrons in the 3p orbital , and atomic radius than N atom. the bond length of P-C of is long than the C-C, as the result the deformation of the local carbon structure [83]. Dan et al. [83] synthesized P-doped carbon from a flake Co-based MOF ($Co_2(H_2O)_2[O_3PCH_2\ (C_6H_4)CH_2\ PO_3]$) by heating and then through HCl acid leaching method. Chunlei Li et al. [84] prepared LFP/C-P electrode with P-doped carbon coated LFP. The value of R_{ct} was 35.5 Ω for LFP/C-P less than LFP/C (371.8 Ω). The Li^+ diffusion coefficient of LFP/C-P

(1.78×10^{-13}cm$^2\cdot$s^{-1}) was improved by 14 % compared with non-P-doped LFP/C (1.56×10^{-13} cm$^2\cdot$s^{-1}). Zhang et al. [85] synthesized phosphorus-doped carbon layers on the particle surface to increase the conductivity of LFP, the charge transfer resistance was significantly reduced by 68.6% from 156.5 Ω to 49.1 Ω and the lithium ion diffusion coefficients increased from 1.15×10^{-13} to 1.72×10^{-13} cm$^2\cdot$s^{-1}. It also showed the excellent rate capability that the discharge capacity was 124.0 mAh$\cdot$g^{-1} at the rate of 20 C.

Similarly, boron doping is the same as nitrogen doping, the size of boron is near to carbon atom and the atom of Boron and carbon can form a strong bond, due to the three valence electrons on the periphery of the boron electron layer [86]. The good natures of B-doped carbon are as follows.

i. The electroneutrality of sp^2 carbon is destroyed and it creates many active sites [87].

ii. B-doped graphene-based materials show enhanced electrical properties [88, 89].

iii. Boron doping increases amounts of hole-type charge carriers and reduce the resistance [90].

Furthermore, Stadie et al. [91] discovered the I_D/I_G decreased with boron content by the direct synthesis route of benzene and boron tribromide in a fully enclosed instrument at elevated temperature. Therefore, the degree of graphitization can be increased by doping with boron in carbon in the method.

Dong et al. [92] synthesized boron-doped carbon coated LFP. The discharge specific capacity of 126.8 mAh$\cdot$g^{-1} at 10 C. At 0.5 C were delivered, the specific capacity reached 160.3 mAh$\cdot$g^{-1}. It was related to its high ion diffusivity and high electrical conductivity. The EIS results showed that charge-transfer resistances of LFP@B-C composites got smaller that of LFP@C composite, and reduced with B content.

The researchers would sometimes dope dual elements to modify the carbon, like nitrogen and phosphorus, boron and nitrogen, etc. Boron and nitrogen co-doped carbon was researched to coat LFP. The coating of N and B co-doped carbon observably enhanced the performance of electrochemical because of the atom of nitrogen and boron provide a large number of electron and hole-type carriers. Zhang et al. [93] reduced the charge transfer resistance of LFP/C-N+B to 1.36×10^{-1} S$\cdot$cm^{-1}, which was much lower than the undoped LFP/C (2.56×10^{-2} S$\cdot$cm^{-1}). By the way, using the negative direction to modified $LiFePO_4$ /C-B with nitrogen (to obtain LFP/C-B+N), the electronic conductivity was only 1.30×10^{-2} S$\cdot$cm^{-1}. Although it had the highest I_D/I_G ratio of 1.30, the dope of boron and nitrogen facilitated more active sites of electrochemical for lithium ion passage, which generally enhance the charge and discharge performance.

Moreover, a large number of stable oxygen on phosphorus groups strengthen the surface wettability of the electrodes, and the improved surface wettability and ion diffusivity are also favorable for the fast reversible redox reactions [94]. Phosphorous-Nitrogen co-doped carbon (P-N-C) materials could directly derive from MOFs. Fu et al. [72] used post synthetic modification (PSM) through one-step pyrolysis to synthesis P-N-C from phosphorus-doped UiO-66-NH_2. However, few studies have reported the nitrogen-phosphorous co-doped carbon to coat lithium iron phosphate. P-N-C modified electrodes may also be interesting in high rate performance.

On the whole, these doped atoms play important roles in carbon. The performances of lithium iron phosphate particles modified with doped carbon are much improved. The doped carbon derived from MOFs is quite convenient to synthesize. One can modify the ligand with substances containing the target atoms or directly choose the suitable metal-organic frameworks that contain the target atoms

to achieve the doped carbon by a simple in-situ heat treatment. Moreover, the double elements co-doped carbon derived from MOFs can be achieved expediently by being infiltrated in a solution containing the target heteroatoms.

5. CONCLUSIONS

The mechanism and pseudocapacitance characteristics of LFP show that the existence of pseudocapacitors may provide a possible direction for the actualization of lithium iron phosphate rapid charge and discharge. For non-coated LFP, the exposure of more (010) face and the greater contact area with the electrolyte often have a great effect on improving its rate performance and specific capacity. The application of carbon in lithium iron phosphate has been extensively researched to enhance the correlation property, including various morphologies of LFP/C composites, carbon sources and dope-carbon etc. Based on the above researches, carbon film thickness, porosity, specific surface area and doped heteroatoms have been proved providing the feasibility of quick charge for the future. Especially, in recent years, the combination of the porous carbon derived from MOFs has been found a new effective way to enhance the electrochemistry performance of charge and discharge for LFP electrode, owing to its controllable pore size and properties, convenient synthesis processing (for example, ZIF-8, MIL-100 and ZIF-67 can be synthesized at room temperature), and in-situ doping with heteroatoms. However, among the existed researches on porous carbon materials at the lithium iron phosphate, there is few literatures on MOFs derived carbon modified lithium iron phosphate. The carbon derived from MOFs has great advantages for mass and electricity transfer and improving the performance of electrode materials. By the way, the central ions of MOFs also play a certain role in carbonized MOFs. For example, there is cobalt in ZIF-67 [95], which can improve the conductivity of carbon [96]. The excellent lithium iron phosphate with appropriate modification will be believed having a lot of good effects on people's life in the near future.

ACKNOWLEDGMENTS
Financial supports from Excellent Young Talents Fund Program of Higher Education Institutions of Anhui Province (gxyqZD2016150), and Key Research and Development Projects in Anhui Province (202004611020033) are acknowledged.

References

1. Y. Park, N. H. Kim, J. Y. Kim, I.-Y. Eom, Y. U. Jeong, M. S. Kim, S. M. Lee, H. C. Choi and Y. M. Jung, *Vib. Spectrosc.*,53 (2010) 60.
2. X. Tian, Z. Chen, Y. Zhu, X. Huang, G. Wu and Y. Zhou, *J. Alloy. Compd.*, 810 (2019).
3. W. Xu, J. Wang, F. Ding, X. Chen, E. Nasybulin, Y. Zhang and J.-G. Zhang, *Energy Environ. Sci.*, 7 (2014)513.
4. A. K. Padhi, K. S. Nanjundaswamy and J. B. Goodenough, *J. Electrochem. Soc.*, 144 (1997) 1188.
5. B. Ellis, W. H. Kan, W. R. M. Makahnouk and L. F. Nazar, *J. Mater. Chem.*, 17 (2007).
6. Y.-S. Hu, Y.-G. Guo, R. Dominko, M. Gaberscek, J. Jamnik and J. Maier, *Adv. Mater.*, 19 (2007)

1963.
7. H. C. Shin, W. I. Cho and H. Jang, *J. Power Sources*, 159 (2006) 1383.
8. N. J. Yun, H. W. Ha and K. H. Jeong, *J. Power Sources*, 160 (2006) 1361.
9. Z. Cao, M. Sang, S. Chen, J. Jia, M. Yang, H. Zhang, X. Li and S. Yang, *Electrochim. Acta*, 333 (2020).
10. Y. Long, Y. Shu, X. Ma and M. Ye, *Electrochim. Acta*, 117 (2014) 105.
11. P. M. Pratheeksha, J. S. Rajeshwari, P. J. Daniel, T. N. Rao and S. Anandan, *J. Nanosci. Nanotechnol.* , 19 (2019) 3002.
12. J. Oh, J. Lee, Y. Jeon, S. Park, J. M. Kim, T. Hwang and Y. Piao, *ACS Sustain. Chem. Eng.*, 7 (2018) 306.
13. F. Yu, J. Zhang, Y. Yang and G. Song, *Electrochim. Acta*, 54 (2009) 7389.
14. T. Nakamura, Y. Miwa, M. Tabuchi and Y. Yamada, *J. Electrochem. Soc.*, 153A1108 (2006).
15. M. S. Whittingham, *Chem. Rev.*, 104 (2004) 4271.
16. H. Lindstrm, S. Sdergren, A. Solbrand, H. Rensmo and S. E. Lindquist, *J. Phys. chem. B*, 101 (1997) 7717.
17. J. W. Kim, V. Augustyn and B. Dunn, *Adv. Energy Mater.* **2**, 141 (2012).
18. X. Wang, G. Li, Z. Chen, V. Augustyn, X. Ma, G. Wang, B. Dunn and Y. Lu, *Adv. Energy Mater.* **1**, 1089 (2011).
19. I. E. Rauda, V. Augustyn, L. C. Saldarriaga-Lopez, X. Chen, L. T. Schelhas, G. W. Rubloff, B. Dunn and S. H. Tolbert, *Adv. Funct. Mater.*, 24 (2015) 6717.
20. V. Augustyn, P. Simon and B. Dunn, *Energy Environ.Sci.*, 7 (2014) 1597.
21. K. Kisu, E. Iwama, W. Naoi, P. Simon and K. Naoi, *Electrochem. Commun.*, 72 (2016) 10.
22. Y. Guan, J. Shen, X. Wei, Q. Zhu, X. Zheng, S. Zhou and B. Xu, *Electrochim. Acta*, 294 (2019) 148.
23. S. Lim, C. S. Yoon and J. Cho, *Chem. Mater.*, 20 (2008) 4560.
24. L. D. Gelb and K. E. Gubbins, *Langmuir*, 14 (1998) 2097.
25. X. Huang, S. Yan, H. Zhao, L. Zhang, R. Guo, C. Chang, X. Kong and H. Han, *Mater. Charact.*, 61 (2010) 720.
26. H. Liu, H. Yang and J. Li, *Electrochim. Acta*, 55 (2010) 1626.
27. Z. Ma, G. Shao, Y. Fan, G. Wang and T. Liu, *Acs Appl. Mater. Interfaces*, 6 (2014) 9236.
28. Y. Zhao, L. Peng, B. Liu and G. Yu, *Nano Lett*, 14 (2014) 2849.
29. J. Zhang, J. Lu, D. Bian, Z. Yang, Q. Wu and W. Zhang, *Ind. Eng. Chem. Res.*, 53 (2014) 12209.
30. Y. Zou, G. Chang, S. Chen, T. Liu, Y. Xia, C. Chen and D. Yang, *Chem. Eng. J.*, 351 (2018) 340.
31. J.Kwang and Kim, *Crystengcomm*, 16 (2014) 2818.
32. X. Zhang, Y. Xia, H. Dou, X. Hao, Y. Wang, B. Ding, S. Dong and J. Wang, *Natl. Sci. Rev.*, 4 (2017) 71.
33. C. Sun, S. Rajasekhara, J. B. Goodenough and F. Zhou, *J. Am. Chem. Soc.*, 133 (2011) 2132.
34. X. F. Wang, Y. Wang, L. Cheng, J. Wu, H. G. Yu and Z. J. Hu,*Journal of Wuhan University of Technology-mater. sci. Ed.*, 4 (2014) 656.
35. G. Du, Y. Xi, X. Tian, Y. Zhu, Y. Zhou, C. Deng, H. Zhu and A. Natarajan, *Ceram. Int.*, 45 (2019) 18247.
36. Y. N. Xu, S. Y. Chung, J. T. Bloking, Y. M. Chiang and W. Y. Ching, *Electrochemical and solid-state letters*, 7 (2004) 881.
37. M. S. A. Sher Shah, A. R. Park, A. Rauf, S. H. Hong, Y. Choi, J. Park, J. Kim, W.-J. Kim and P. J. Yoo, *RSC Adv.*, 7 (2017) 3125.
38. P. Bai and M. Z. Bazant, *Nat. Commun.*, 5 (2014) 3585
39. T. Gao, C. Xu, R. Li, R. Zhang, B. Wang, X. Jiang, M. Hu, Y. Bando, D. Kong, P. Dai and X. B. Wang, *ACS Nano*, 13 (2019) 11901.
40. J. L. C. Rowsell and O. M. Yaghi, *Microporous Mesoporous Mat.*, 73 (2004) 3.
41. F. Guo, Z. Kong, T. Wang, X. Liu, Z. Xu, A. Fu, Y. Li, P. Guo, Y. G. Guo and H. Li, *Ionics*, 26 (2020) 2737.

42. S. Weng, T. Huo, K. Liu, J. Zhang and W. Li, *J. Alloy. Compds.*, 818 (2020) 152858.
43. X. Tian, W. Chen, Z. Jiang and Z.-J. Jiang, *Ionics*, 26 (2020) 2715.
44. Q. Fan, Y. Zhang, Q. Xu, J. Wang, L. Lei, Y. Sun and P. D. Lund, *Energy Storage Materials*, 21 (2019) 457.
45. J. Xia, F. Zhu, L. Wang, G. Wang, Y. Meng and Y. Zhang, *J. Nanopart. Res.*, 20 (2018) 2.
46. Y. Yan, Q. Li, B. Ren, R. Yang, Y. Xu, L. Zhong and H. Wu, *Ionics*, 24 (2017) 671.
47. G. Du, Y. Zhou, X. Tian, G. Wu, Y. Xi and S. Zhao, *Appl. Surf. Sci.*, 453 (2018) 493.
48. X. Yi, F. Zhang, B. Zhang, W. J. Yu, Q. Dai, S. Hu, W. He, H. Tong, J. Zheng and J. Liao, *Ceram. Int.*, 44 (2018) 18181.
49. X. Xu, Z. Hao, H. Wang, Y. Xie, J. Liu and H. Yan, *J. Mater. Sci.-Mater. Electron.*, 29 (2018) 16630.
50. Y. Cai, D. Huang, Z. Ma, H. Wang, Y. Huang, X. Wu and Q. Li, *Electrochim. Acta*, 305 (2019) 563.
51. W. Bao, A. K. Mondal, J. Xu, C. Wang, D. Su and G. Wang, *J. Power Sources*, 325 (2016) 286.
52. Z. S. Wu, K. Parvez, X. Feng and K. Mullen, *Nat. Commun.*, 4 (2013) 2487.
53. Y. Wang, Y. Zhang, G. Wang, X. Shi, Y. Qiao, J. Liu, H. Liu, A. Ganesh and L. Li, *Adv. Funct. Mater.*, 30 (2020) 7284.
54. L. T. N. Huynh, T. T. D. Tran, H. H. A. Nguyen, T. T. T. Nguyen, V. M. Tran, A. Grag and M. L. P. Le, *J. Solid State Electrochem.*,18 (2018) 3934.
55. F. Leroux, K. Metenier, S. Gautier, E. Frackowiak and S. Bonnamy, *J.Power Sources*, s81–82 (1999) 317.
56. E. Frackowiak, *carbon*, 37 (1999) 61.
57. B. Lung-Hao Hu, F. Y. Wu, C. T. Lin, A. N. Khlobystov and L. J. Li, *Nat. Commun.*, 4 (2013) 1687.
58. W. Xing-Long, J. Ling-Yan, C. Fei-Fei, G. Yu-Guo and W. Li-Jun, *Adv. Mater.*, 21 (2009) 2710.
59. Z. W. Xiao, Y. J. Zhang and G. R. Hu, *J. Cent. South Univ.*, 22 (2015) 4507.
60. H. P. Liu, Z. X. Wang, X. H. Li, H. J. Guo, W. J. Peng, Y. H. Zhang and Q. Y. Hu, *J. Power Sources*, 184 (2008) 469.
61. S. Wi, S. Nam, Y. Oh, J. Kim, H. Choi, S. Hong, S. Byun, S. Kang, D. J. Choi, K. O. Ahn, Y. H. Kim and B. Park, *J. Nanopart. Res.*, 14 (2012) 1327.
62. S. A. Hong, A. Nugroho, S. J. Kim, J. Kim, K. Y. Chung, B. W. Cho and J. W. Kang, *Res. Chem. Intermed.*, 37 (2011) 429.
63. Y. Mo, J. Liu, C. Meng, M. Xiao, S. Ren, L. Sun, S. Wang and Y. Meng, *carbon*, 147 (2019) 19.
64. Y. Zhou, C. D. Gu, J. P. Zhou, L. J. Cheng, W. L. Liu, Y. Q. Qiao, X. L. Wang and J. P. Tu, *Electrochim. Acta*, 56 (2011) 5054.
65. L. Sun, Q. Deng, B. Fang, Y. Li, L. Deng, B. Yang, X. Ren and P. Zhang, *Crystengcomm*, 18 (2016) 7537.
66. Y. D. Cho, G. T. K. Fey and H. M. Kao, *J. Power Sources*, 189 (2009) 256.
67. S. Flandrois and B. Simon, *carbon*, 37 (1999) 165.
68. L. T. N. Huynh, H. H. A. Nguyen, T. T. D. Tran, T. T. T. Nguyen, T. M. A. Nguyen, T. H. La, V. M. Tran and M. L. P. Le, *J. Nanomater.*, 2019 (2019) 1.
69. X. Xu, C. Qi, Z. Hao, H. Wang, J. Jiu, J. Liu, H. Yan and K. Suganuma, *Nanomicro. Lett.*, 10 (2018) 1.
70. Y. Liu, J. Gu, J. Zhang, F. Yu, L. Dong, N. Nie and W. Li. *J. Power Sources*, 304 (2016) 42.
71. S. Yuan, L. Feng, K. Wang, J. Pang, M. Bosch, C. Lollar, Y. Sun, J. Qin, X. Yang, P. Zhang, Q. Wang, L. Zou, Y. Zhang, L. Zhang, Y. Fang, J. Li and H. C. Zhou, *Adv. Mater.*,30 (2018) e1704303.
72. Y. A. Fu, Y. Huang, Z. Xiang, G. Liu and D. Cao, *Eur. J. Inorg. Chem.*, 2016 (2016) 2100.
73. Z. Luo, S. Lim, Z. Tian, J. Shang, L. Lai, B. Macdonald, C. Fu, Z. Shen, T. Yu and J. Lin, *J. Mater. Chem.*, 21 (2011) 8038.
74. J. Li, X. Li, P. Zhao, D. Y. Lei, W. Li, J. Bai, Z. Ren and X. Xu, *carbon*, 84 (2015) 460.
75. Z. Shen, Y. Mo, J. Du and A. Chen, *Appl. Surf. Sci.*, 527 (2020) 146845.
76. F. Zheng, Y. Yang and Q. Chen, *Nat. Commun.*, 5 (2014) 5261.

77. U. P. Azad, S. Ghosh, C. J. Verma, A. K. Singh, A. K. Singh and R. Prakash, *ChemistrySelect*, 3 (2018) 6107.
78. F. Wang, H.-Y. Zhuo, X. Han, W.-M. Chen and D. Sun, *J. Mater. Chem. A.*, 5 (2017) 22964.
79. Z. Ding, L. Zhao, L. Suo, Y. Jiao, S. Meng, Y. Hu, Z. Wang and L. Chen, *Phy. Chem. Chem. Phys.*, 13 (2011) 15127.
80. G. A. Ferrero, A. B. Fuertes and M. A. Sevilla, *J. Mater. Chem. A.*, 3 (2015) 2914.
81. L. Sun, C. Tian, Y. Fu, Y. Yang, J. Yin, L. Wang and H. Fu, *chem.-eur.j.*, 20 (2014) 564
82. J. Ou, L. Yang, F. Jin, S. Wu and J. Wang, *Adv. Powder Technol.*, 31 (2020) 1220.
83. D. Xu, Q. Ding, J. Li, H. Chen, Y. Pan and J. Liu, *Inorg. Chem. Commun.*, 119 (2020) 108141.
84. C. Li, Y. Xie, N. Zhang, L. Ai, Y. Liang, K. Tuo, X. Ye, G. Jia and S. Li, *Ionics*, 25 (2018) 927.
85. J. Zhang, J. Wang, Y. Liu, N. Nie, J. Gu, F. Yu and W. Li, *J. Mater. Chem. A.*, 3 (2015) 2043.
86. T. Wu, H. Shen, L. Sun, B. Cheng, B. Liu and J. Shen, *New J. Chem.*, 36 (2012) 1385.
87. Y. Zhao, L. Yang, S. Chen, X. Wang, Y. Ma, Q. Wu, Y. Jiang, W. Qian and Z. Hu, *J. Am. Chem. Soc.*, 135 (2013) 1201.
88. J. Han, L. Zhang, S. Lee, J. Oh, K. Lee, J. R. Potts, J. Ji, X. Zhao, R. S. Ruoff and S. Park, *ACS nano*, 7 (2013) 19.
89. Y. A. Kim, K. Fujisawa, H. Muramatsu, T. Hayashi, M. Endo, T. Fujimori, K. Kaneko, M. Terrones, J. C. Behrends and A. J. Eckmann, *ACS nano*, 6 (2012) 6293.
90. L. S. Panchakarla, K. S. Subrahmanyam, S. K. Saha, A. Govindaraj, H. R. Krishnamurthy, U. V. Waghmare and C. N. R. Rao, *Adv. Mater.*, 21 (2009) 4726.
91. N. P. Stadie, E. Billeter, L. Piveteau, K. V. Kravchyk, M. Döbeli and M. V. Kovalenko, *Chem. Mat.*, 29 (2017) 3211.
92. J. Feng and Y. Wang, *Appl. Surf. Sci.*, 390 (2016) 481.
93. J. Zhang, N. Nie, Y. Liu, J. Wang, F. Yu, J. Gu and W. Li, *ACS Appl. Mater. Interfaces*, 7 (2015) 20134.
94. X. Yan, Y. Liu, X. Fan, X. Jia, Y. Yu and X. Yang, *J. Power Sources*, 248 (2014) 745.
95. J. Qian, F. Sun and L. Qin, *Mater. Lett.*, 82 (2012) 220.
96. S. Li, S. Peng, L. Huang, X. Cui, A. M. Al-Enizi and G. Zheng, *ACS Appl. Mater. Interfaces*, 8 (2016) 20534